Synthesis and characterization of a family of tetranuclear manganese(III) phosphonate complexes†‡

Mei Wang,[ab] Chengbing Ma,[a] Daqiang Yuan,[a] Mingqiang Hu,[ab] Changneng Chen*[a] and Qiutian Liu[a]

Received (in Montpellier, France) 1st May 2007, Accepted 11th July 2007
First published as an Advance Article on the web 15th August 2007
DOI: 10.1039/b706514k

Four tetranuclear manganese(III) complexes containing phosphonate ligands (RPO_3^{2-}, R = Me, Et and *n*-Bu), $[Mn_4O_2(MePO_3)_2(O_2CMe)_4(bpy)_2]\cdot 4MeCOOH$ (**1**), $[Mn_4O_2(EtPO_3)_2(O_2CMe)_4(bpy)_2]\cdot 7H_2O$ (**2**), $[Mn_4O_2(n\text{-}BuPO_3)_2(O_2CMe)_4(bpy)_2]\cdot 4H_2O\cdot(COOH)_2$ (**3**) and $[Mn_4O_2(MePO_3)_2(O_2CPh)_4(phen)_2]\cdot 4PhCOOH\cdot 2MeCN$ (**4**), have been synthesized and characterized by IR spectroscopy, ESI-MS spectrometry, electrochemical analysis, magnetic measurements and TGA. The X-ray analysis shows that the four complexes all have one $[Mn_4(\mu_3\text{-}O)_2]^{8+}$ core with four coplanar Mn atoms disposed in an extended "butterfly-like" arrangement and two O atoms triply bridging each "wing", and the peripheral ligation is provided by four μ_2-$MeCO_2^-$ or four μ_2-$PhCO_2^-$, two terminal bpy or phen (bpy = 2,2′-bipyridine, phen = 1,10-phenanthroline) groups at both ends of the molecule, and two bicapping μ_3-phosphonate ligands, which each binds to three manganese centers above and below the plane. The cyclic voltammetry of **1** and **3** each displays four reduction and one oxidation processes, of which the four reduction processes are possibly attributed to the reduction of four Mn^{III} of the compounds to Mn^{II}. The ESI-MS data indicate that the family of complexes are stable in solution. Magnetic susceptibility measurements reveal that compounds **1** and **3** display antiferromagnetic interactions between the adjacent Mn^{III} ions mediated through the μ_3-O, O–C–O and O–P–O bridges.

Introduction

In the past few decades many tetranuclear manganese complexes have been synthesized and characterized due to two main reasons: bioinorganic chemistry and magnetic materials. For the first reason, it is believed that the site for water oxidation in the photosynthetic apparatus of green plants and cyanobacteria contains a tetranuclear manganese aggregate operating on the donor side of Photosystem II (PS II).[1] The synthesis and structure characterization of manganese complexes have provided a wealth of data to model the Mn_4 water oxidation center (WOC).[2] The second reason is to design new single-molecule magnets (SMMs).[3] SMMs are regarded as the elementary units in both ultimate high-density magnetic storage and the design of quantum computers.[4,5] Accompanying peculiar physical phenomena, such as very slow magnetization relaxation rate and quantum-tunneling of the magnetization,[6,7] also make manganese clusters objects of both technological and fundamental scientific interest.[8]

Phosphonates are a family of ligands that have three O donors which can bind to metal ions. Transition-metal phosphonate complexes have received a lot of attention in recent years primarily because of their potential applications in catalysis, ion exchange, proton conductivity, intercalation chemistry, photochemistry and material chemistry.[9–12] Several metal phosphonate compounds that contain vanadium,[13] aluminium,[14] copper,[15,16] cobalt,[8] zinc,[16–18] cadmium,[19] and iron[20] have been prepared so far. Recently utilization of the phosphonate to prepare polynuclear manganese complexes has received an increasing attention, and three kinds of target clusters with higher nuclearity, one hexa-, one icosa- and one dodeca-nuclear manganese aggregate have been obtained using bulky phosphonates (phenylphosphonate, benzylphosphonate and cyclohexenephosphonate) as ligands.[8,21,22] However, smaller manganese clusters, *e.g.* the tetranuclear manganese complexes with phosphonate ligands remain relatively scarce.[23] Here we report the synthesis, structures, electrochemistry and magnetic properties of a family of Mn_4 complexes with smaller and various phosphonate ligands, $[Mn_4O_2(MePO_3)_2(O_2CMe)_4(bpy)_2]\cdot 4MeCOOH$ (**1**), $[Mn_4O_2(EtPO_3)_2(O_2CMe)_4(bpy)_2]\cdot 7H_2O$ (**2**), $[Mn_4O_2(n\text{-}BuPO_3)_2(O_2CMe)_4(bpy)_2]\cdot 4H_2O\cdot(COOH)_2$ (**3**) and $[Mn_4O_2(MePO_3)_2(O_2CPh)_4(phen)_2]\cdot 4PhCOOH\cdot 2MeCN$ (**4**).

[a] *State Key Laboratory of Structural Chemistry, Fujian Institute of Research on the Structure of Matter, The Chinese Academy of Sciences, Fuzhou, Fujian, 350002, China. E-mail: ccn@fjirsm.ac.cn; Fax: +86 591 83792395*
[b] *Graduate School of the Chinese Academy of Sciences, Beijing, 100039, China*

† Electronic supplementary information (ESI) available: Details of the packing diagram of compound **2**, differential pulse voltammetry for complex **1**, ESI-MS spectrum of complex **1**, cyclic voltammogram for complex **3**, differential pulse voltammetry for complex **3** and TG curves of compounds **1** and **3**. See DOI: 10.1039/b706514k
‡ The HTML version of this article has been enhanced with colour images.

Results and discussion

Synthesis

Previous work had proved that $NBu^n_4MnO_4$ in nonaqueous solvents represents a useful route to forming higher oxidation state Mn complexes.[24,25] The preparation of the four compounds **1–4** resulted from the comproportionation reaction between Mn^{2+} and $NBu^n_4MnO_4$ in MeCN–MeOH or CH_2Cl_2–MeCN–MeOH. The average Mn oxidation state in all of the reactions is +3, so the formation of $4Mn^{III}$ products can be achieved. The Mn^{II} : Mn^{VII} ratio employed was 4 : 1, as required for a desired Mn^{III}_4 product according to [eqn (1)],

$$4\,Mn^{II} + Mn^{VII} \rightarrow 5/4\,Mn^{III}_4 \qquad (1)$$

The reaction of $Mn(O_2CMe)_2 \cdot 4H_2O$, $NBu^n_4MnO_4$, MeCOOH and 2,2′-bipyridine with methanephosphonic acid ($MePO_3H_2$) produced a deep brown solution, from which compound **1** was obtained. The experimental procedures for the preparation of compounds **2–4** are similar but differing in phosphonic acid, carboxylic acid and N-containing coligands. Compounds **1–3** crystallized in a mixed solvent of MeCN–MeOH, while compound **4** crystallized in a mixed solvent of CH_2Cl_2–MeCN–MeOH. Compounds **1–4** with analogous structures can not be obtained by the same synthesis method, which might be due to the difference of the solubility and acidity of the reagents. Also we can not obtain large clusters with these phosphonate ligands (RPO_3^{2-}, R = Me, Et and *n*-Bu) possibly because these ligands are relatively small.

Description of the crystal structures

The ORTEP diagrams for complexes **1**, **2**, **3** and **4** are shown in Fig. 1–4, respectively. The crystallographic data for **1–4** are summarized in Table 1. Selected bond lengths and angles for all of the four structures are given in Table 2.

The four manganese atoms are all Mn^{III} ions according to the bond valence sum calculations.[26] The four complexes all lie about inversion centers. All the four complexes possess an $[Mn_4(\mu_3\text{-}O)_2]^{8+}$ core, with the four coplanar Mn atoms disposed in an extended "butterfly-like" arrangement. The core structure can be considered as two Mn_3O triangular units, which consist of Mn(1), Mn(1A), Mn(2) and μ_3-O(1), and

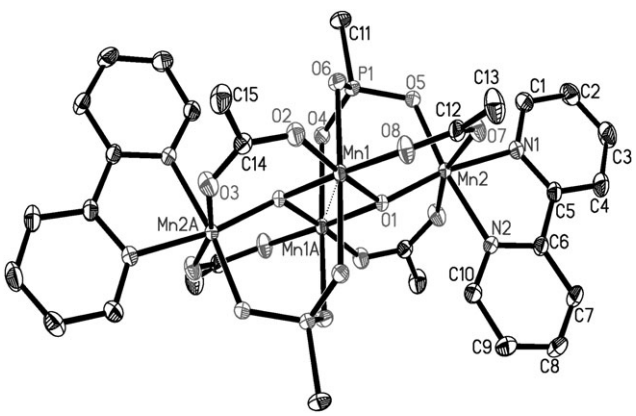

Fig. 1 Crystal structure of **1** at 30% probability displacement ellipsoids (hydrogen atoms have been omitted for clarity). Symmetry code A: $-x + 3/2, -y + 1/2, -z + 1$.

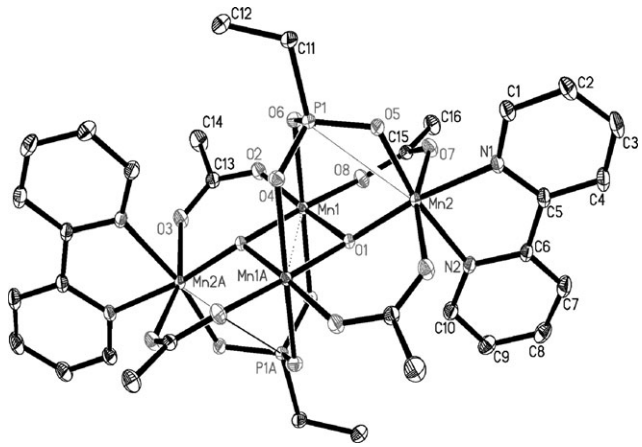

Fig. 2 Crystal structure of **2** at 30% probability displacement ellipsoids (hydrogen atoms have been omitted for clarity). Symmetry code A: $-x + 2, -y, -z + 1$.

Mn(1), Mn(1A), Mn(2A) and μ_3-O(1A), joined together by sharing Mn(1)···Mn(1A) as the same edge. There are two bicapping μ_3-phosphonate ligands above and below the Mn_4 plane, which each bind to three manganese centers of the Mn_3O triangular unit (Fig. 5). The distances between the two planes formed by {O(4)–O(5)–O(6)} and {Mn(1)–Mn(2)–Mn(1A)–Mn(2A)} of **1–4** are 2.0451, 1.9878, 2.0134 and 2.0375 Å, respectively. The distances of P(1)···P(1A) are 5.781, 5.733, 5.756 and 5.814 Å, respectively. The Mn(1)···Mn(1A) bond lengths of **1–4** (2.8722(7), 2.8466(7), 2.8419(11) and 2.8582(5) Å) are all much shorter than the distances of Mn(2)···Mn(1) (3.362(4), 3.355(4), 3.365(2), 3.325(3) Å), which are comparable to those of complexes with similar cores reported before.[27–30] This is in agreement with the number of bridging oxides. It is stated that the Mn···Mn distances in oxide-bridged systems are about

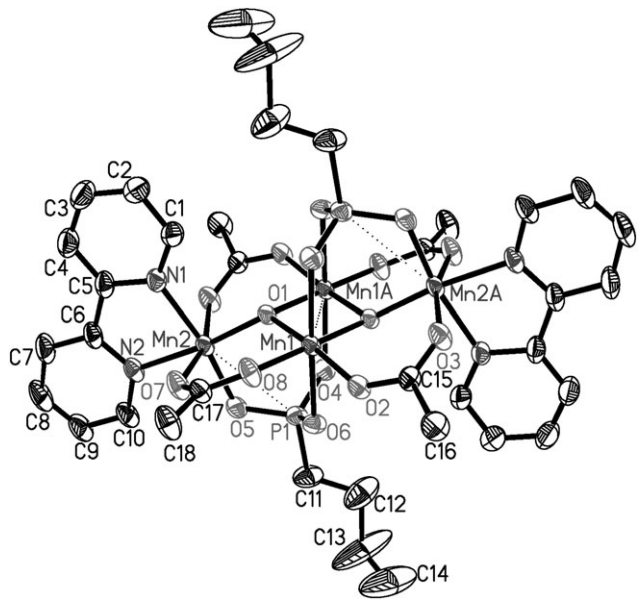

Fig. 3 Crystal structure of **3** at 30% probability displacement ellipsoids (hydrogen atoms have been omitted for clarity). Symmetry code A: $-x, -y + 2, -z$.

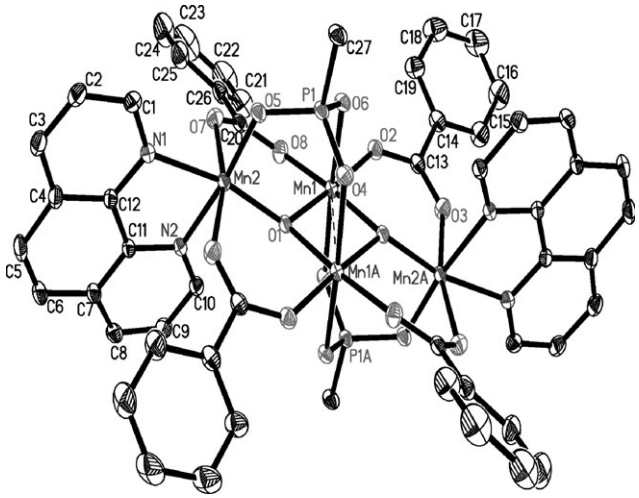

Fig. 4 Crystal structure of **4** at 30% probability displacement ellipsoids (hydrogen atoms have been omitted for clarity). Symmetry code A: $-x + 1, -y + 1, -z$.

2.7 ~ 2.8 Å if bridged by two oxides and about 3.3 Å if bridged by one oxide.[31] Unlike the Mn_3O complexes,[24,32,33] the two μ_3-O atoms are not in the plane of the four Mn atoms but 0.3593, 0.3962, 0.3859, 0.3628 Å below and above the plane for **1**, **2**, **3** and **4**, respectively. In addition to two bicapping phosphonate ligands, there are a total of four bridging μ_2-$MeCO_2^-$ or μ_2-$PhCO_2^-$ groups around the four Mn atoms, two terminal bpy or phen groups located at two ends of the molecule, giving a six-coordinate near-octahedral geometry around each Mn^{III} center. The six-coordinate Mn atoms show Jahn–Teller distortion, for the Mn(III) site with high-spin d^4 configuration in the compounds, which gives rise to the elongation along the axes O(6)–Mn(1)–O(4A) and O(6A)–Mn(1A)–O(4) composed of phosphonate oxygen atoms, Mn(1) and Mn(1A). The Mn(1)–O(6) and Mn(1)–O(4A) bond distances (2.2746(17) and 2.2199(17) Å for **1**, 2.2016(14) and 2.2074(14) Å for **2**, 2.246(3) and 2.197(3) Å for **3**, 2.2788(12) and 2.2262(13) Å for **4**, respectively) are much longer than the other Mn–O bond distances in the respective complexes.

As listed in Table 3, seven hydrogen bonds are found in compound **2**. One solvate H_2O molecule donates its hydrogen atoms H(10B) and H(10C) to one phosphonate oxygen O(6) and one acetate oxygen O(2), respectively, to form two hydrogen bonds, O(10)–H(10B)···O(6) and O(10)–H(10C)···O(2). Another solvate H_2O molecule donates its hydrogen atoms H(9B) and H(9C) to phosphonate oxygen O(4) and solvate water oxygens O(12) (occupancy factor 0.5) and O(12&) (occupancy factor 0.5) to form three hydrogen bonds, O(9)–H(9B)···O(4), O(9)–H(9C)···O(12) and O(9)–H(9C)···O(12&) ($-x, -y + 3, -z$). The solvate H_2O molecule (O(11)) bridges solvate H_2O molecules (O(10) and O(9#)) through two hydrogen bonds, O(11)–H(11D)···O(10) and O(11)–H(11C)···O(9#) ($-x + 1, -y + 2, -z + 1$) to form 1D zigzag chains. (Fig. 6 and Fig. S1, ESI†).

Electrochemical studies

The cyclic voltammetry (CV) and differential pulse voltammetry (DPV) of **1** and **3** have been recorded in distilled MeCN solution under argon. The CV and DPV of compound **1** (Fig. 7 and Fig. S2, ESI†) show that, when scanning towards cathodic potential, four reduction processes at *ca.* −0.911, −1.69, −2.12 and −2.42 V *vs.* Ag/AgCl are observed. One oxidation response at *ca.* −1.94 V *vs.* Ag/AgCl is observed when scanning towards anodic potential. During scanning towards cathodic potential, the four reduction processes are possibly attributed to the reduction of four Mn^{III} of compound **1** to Mn^{II}. These values are more negative than those reported for other complexes with the $[Mn_4O_2]^{8+}$ core.[28,34] The more negative reduction potential values indicate that this family of tetranuclear manganese(III) complexes containing phosphonate ligands are more difficult to be reduced. The reduction and oxidation peaks at –2.12 and −1.94 V seem to be reversible waves. The changes in the reduction and oxidation processes at the scan rate range of 50–500 mV were studied in the potential range from −1.8 to −2.25 V. As shown in the inset of Fig. 7, ΔE_p increases slightly as the scan rate increases, suggesting that this process is quasi-reversible. The ESI-MS spectrum (positive mode) of an acetonitrile solution of **1** gave one major peak at m/z 1013.6 (Fig. S3, ESI†), which

Table 1 Crystallographic data summary for complexes **1–4**

	1	**2**	**3**	**4**
Empirical formula	$C_{38}H_{50}Mn_4N_4O_{24}P_2$	$C_{32}H_{52}Mn_4N_4O_{23}P_2$	$C_{38}H_{54}Mn_4N_4O_{24}P_2$	$C_{86}H_{72}Mn_4N_6O_{24}P_2$
Formula weight	1228.52	1142.48	1232.55	1855.20
Space group	$C2/c$	$P\bar{1}$	$P\bar{1}$	$P2_1/n$
a/Å	17.8554(9)	10.080(3)	11.4387(14)	18.0431(7)
b/Å	15.7085(9)	11.084(3)	11.4850(12)	11.0649(3)
c/Å	17.7912(9)	11.559(3)	11.9747(11)	21.7461(9)
α/°	90	64.798(5)	100.4590(10)	90
β/°	96.224(3)	81.789(7)	103.024(4)	91.002(2)
γ/°	90	82.715(6)	113.282(3)	90
V/Å^3	4960.7(5)	1153.4(6)	1342.0(2)	4340.8(3)
Z	4	1	1	2
T/K	293(2) K	293(2)	293(2)	293(2)
λ(Mo-Kα)/Å	0.71073	0.71073	0.71073	0.71073
D_c/g cm^{-3}	1.645	1.645	1.525	1.419
μ/mm^{-1}	1.147	1.225	1.060	0.683
R^a	0.0400	0.0316	0.0558	0.0409
wR^b	0.1101	0.0855	0.1564	0.1143

^{a} $R = \sum||F_o| - |F_c||/\sum|F_o|$. ^{b} $wR = [\sum w(|F_o| - |F_c|)^2/\sum wF_o^2]^{1/2}$.

Table 2 Selected bond lengths (Å) and angles (°) for **1–4**

	1	2	3	4
Mn(1)–O(1)	1.9115(16)	1.9152(13)	1.914(2)	1.8876(12)
Mn(1)–O(1A)[a]	1.9245(15)	1.9277(12)	1.918(2)	1.9292(12)
Mn(1)–O(8)	1.9341(17)	1.9662(14)	1.947(3)	1.9526(14)
Mn(1)–O(2)	1.9368(18)	1.9556(14)	1.945(3)	1.9204(13)
Mn(1)–O(4A)	2.2199(17)	2.2074(14)	2.197(3)	2.2262(13)
Mn(1)–O(6)	2.2746(17)	2.2016(14)	2.246(3)	2.2788(12)
Mn(1)···Mn(1A)	2.8722(7)	2.8466(7)	2.8419(11)	2.8582(5)
Mn(2)–O(1)	3.3618(5)	1.8640(12)	1.863(2)	1.8612(12)
Mn(2)–O(5)	1.8572(15)	1.8769(13)	1.870(3)	1.8761(13)
Mn(2)–N(1)	1.9044(16)	2.0497(16)	2.059(4)	2.0652(16)
Mn(2)–N(2)	2.054(2)	2.0655(16)	2.051(3)	2.0555(15)
Mn(2)–O(3A)	2.0579(19)	2.1942(15)	2.186(3)	2.1831(15)
Mn(2)–O(7)	2.1653(18)	2.1896(15)	2.167(3)	2.1963(15)
O(1)–Mn(1)–O(1A)	83.04(7)	84.41(5)	84.27(11)	83.03(5)
O(1)–Mn(1)–O(8)	96.20(7)	96.75(6)	97.06(12)	95.35(6)
O(1A)–Mn(1)–O(8)	177.55(8)	176.09(5)	177.92(11)	175.37(6)
O(1)–Mn(1)–O(2)	176.00(8)	175.64(6)	173.28(11)	176.00(6)
O(1A)–Mn(1)–O(2)	97.84(7)	95.84(6)	95.55(11)	98.16(6)
O(8)–Mn(1)–O(2)	83.08(8)	83.29(6)	83.32(12)	83.76(6)
O(1)–Mn(1)–O(4A)	87.87(7)	87.53(5)	88.38(10)	88.55(5)
O(1A)–Mn(1)–O(4A)	86.47(6)	87.37(5)	87.37(10)	85.98(5)
O(8)–Mn(1)–O(4A)	91.17(8)	88.95(6)	91.07(12)	89.65(6)
O(2)–Mn(1)–O(4A)	96.07(8)	96.83(6)	98.33(11)	95.34(6)
O(1)–Mn(1)–O(6)	86.26(6)	86.35(5)	86.38(10)	86.54(5)
O(1A)–Mn(1)–O(6)	87.13(6)	87.50(5)	86.51(11)	86.51(5)
O(8)–Mn(1)–O(6)	95.15(8)	96.29(6)	95.16(12)	97.74(6)
O(2)–Mn(1)–O(6)	89.88(7)	89.30(6)	86.90(11)	89.71(5)
O(4A)–Mn(1)–O(6)	171.80(6)	172.37(5)	172.31(10)	171.48(5)
O(1)–Mn(2)–O(5)	94.94(7)	96.52(6)	96.11(11)	95.82(5)
O(1)–Mn(2)–N(1)	170.77(7)	172.43(6)	94.24(12)	168.29(6)
O(5)–Mn(2)–N(1)	93.55(8)	90.87(6)	169.63(13)	93.38(6)
O(1)–Mn(2)–N(2)	93.05(7)	93.95(6)	173.19(13)	90.97(6)
O(5)–Mn(2)–N(2)	171.99(8)	168.95(6)	90.67(14)	173.00(6)
N(1)–Mn(2)–N(2)	78.51(8)	78.78(7)	78.98(14)	80.12(6)
O(1)–Mn(2)–O(3A)	94.52(7)	93.52(6)	94.32(10)	92.52(6)
O(5)–Mn(2)–O(3A)	95.77(8)	99.06(6)	95.65(14)	95.55(6)
N(1)–Mn(2)–O(3A)	81.03(7)	83.66(6)	82.85(13)	79.36(6)
N(2)–Mn(2)–O(3A)	84.05(8)	83.79(6)	84.40(12)	85.85(6)
O(1)–Mn(2)–O(7)	96.27(7)	95.37(6)	94.64(11)	98.20(6)
O(5)–Mn(2)–O(7)	93.97(8)	93.98(6)	95.09(14)	92.16(6)
N(1)–Mn(2)–O(7)	86.72(7)	85.72(6)	84.75(14)	88.66(6)
N(2)–Mn(2)–O(7)	84.68(8)	81.49(6)	85.31(12)	85.15(6)
O(3A)–Mn(2)–O(7)	164.78(7)	163.27(6)	165.19(13)	166.10(6)

[a] Symmetry transformations used to generate equivalent atoms: (**1**) A: $-x + 3/2, -y + 1/2, -z + 1$; (**2**) A: $-x + 2, -y, -z + 1$; (**3**) A: $-x, -y + 2, -z$; (**4**) A: $-x + 1, -y + 1, -z$.

corresponds to $[\mathbf{1} + Na]^+$, suggesting the complex is stable in solution. As shown in Fig. 7 and Fig. S4, ESI†, compounds **1** and **3** displayed similar electrochemical features but different potentials. The CV and DPV of compound **3** (Fig. S4 and S5, ESI†) show that, when scanning towards cathodic potential, four reduction processes at *ca.* −0.861, −1.32, −2.11 and −2.42 V *vs.* Ag/AgCl are observed. One oxidation response at *ca.* −2.02 V *vs.* Ag/AgCl is observed when scanning towards anodic potential.

Magnetic properties

The variable-temperature magnetic susceptibility data of complexes **1** and **3** were collected in the temperature range 2–300 K under a field of 0.5 T, and the resulting plots of χ_M and $\chi_M T$ *vs.* T are depicted in Fig. 8 and Fig. 9. The $\chi_M T$ per Mn_4 at room temperature are 8.15 $cm^3\ mol^{-1}$ K for **1** and 8.63 $cm^3\ mol^{-1}$ K for **3**, which are smaller than that of 12.01 $cm^3\ mol^{-1}$ K expected for four independent Mn(III) ions with $S = 2$. Upon cooling, the values of $\chi_M T$ gradually decrease to 4.61 $cm^3\ mol^{-1}$ K for **1** and 5.08 $cm^3\ mol^{-1}$ K for **3** at 20 K, whereupon the values fall sharply to 0.71 $cm^3\ mol^{-1}$ K for **1** and 0.86 $cm^3\ mol^{-1}$ K for **3** at 2 K, respectively. This result indicates the overall antiferromagnetic character of the system. The susceptibility data were fitted over the full temperature range based on the interaction pattern shown in Fig. 10 and on the corresponding Hamiltonian [eqn (2)].

$$\hat{H} = -2J_1(\hat{S}_1\hat{S}_2 + \hat{S}_1\hat{S}_3 + \hat{S}_2\hat{S}_4 + \hat{S}_3\hat{S}_4) - 2J_2\hat{S}_1\hat{S}_4 - D(\hat{S}_{1z}^2 + \hat{S}_{2z}^2 + \hat{S}_{3z}^2 + \hat{S}_{4z}^2) \quad (2)$$

The fitted parameters obtained with this computing model are $J_1 = -0.589\ cm^{-1}$, $J_2 = -2.73\ cm^{-1}$, $g = 1.969$, $D = 2.566\ cm^{-1}$ and $R = 3.632 \times 10^{-5}$ (defined as $\sum[(\chi_M T)_{calc} - (\chi_M T)_{obs}]^2/[\sum(\chi_M T)_{obs}]^2$) for **1** and $J_1 = -0.601\ cm^{-1}$, $J_2 = -3.078\ cm^{-1}$, $g = 2.040$, $D = 2.403\ cm^{-1}$ and $R = 2.506 \times$

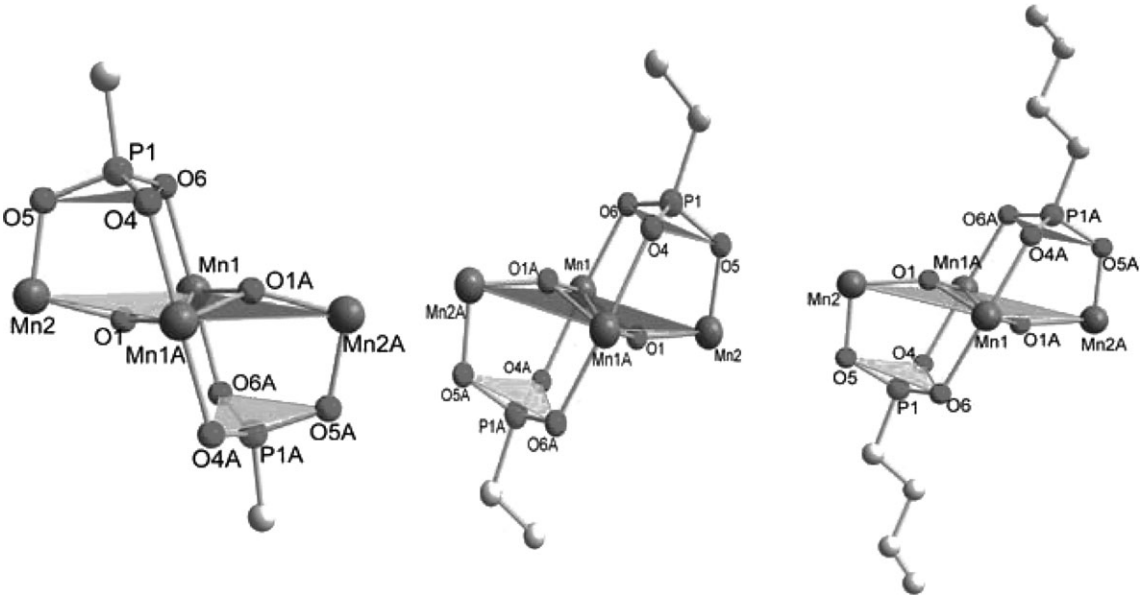

Fig. 5 DIAMOND view of **1**, **2** and **3** showing the planar parallelogram Mn4 array bicapped by the $[MePO_3]^{2-}$, $[EtPO_3]^{2-}$, $[n\text{-}BuPO_3]^{2-}$, respectively. The other ligands have been removed for clarity.

Table 3 Hydrogen bond distances (Å) and angles (°) for compound **2**

D–H···A	*d*(D–H)	*d*(H···A)	∠DHA	*d*(D···A)	Symmetry code
O(9)–H(9B)···O(4)	0.874	2.002	177.57	2.875	
O(9)–H(9C)···O(12)	0.886	1.885	163.00	2.745	
O(9)–H(9C)···O(12&)	0.886	2.230	125.86	2.841	$-x, -y + 3, -z$
O(10)–H(10B)···O(6)	0.880	1.958	165.80	2.820	
O(10)–H(10C)···O(2)	0.871	2.348	132.39	3.004	
O(11)–H(11C)···O(9#)	0.886	1.910	151.33	2.721	$-x + 1, -y + 2, -z + 1$
O(11)–H(11D)···O(10)	0.844	2.070	154.47	2.854	

10^{-5} for **3**. Although this set of parameters fit the experimental data well, they are not realistic because the tetragonally elongated Mn(III) complexes with Jahn–Teller distortion might not have so large and positive *D* parameter.[35] Thus we obtained another set of fitted parameters by introducing the intercomplex interactions based on molecular field approximation zJ' ($\chi = \chi_0/[1 - \chi_0(2zJ'/Ng^2\mu_B{}^2)]$).[36] Based on the Hamiltonian with $D = 0$ [eqn (2)], the fitted parameters above

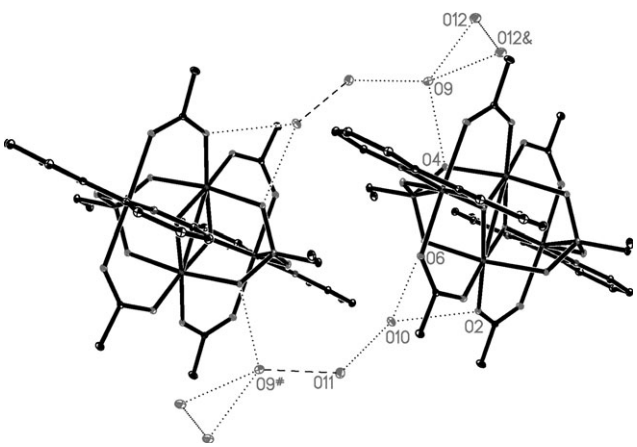

Fig. 6 A view of symmetric dimer of compound **2** produced by the solvate water molecules. Atoms labelled with a ampersand (&) or hash (#) are at the symmetry positions ($-x, -y + 3, -z$) and ($-x + 1, -y + 2, -z + 1$), respectively.

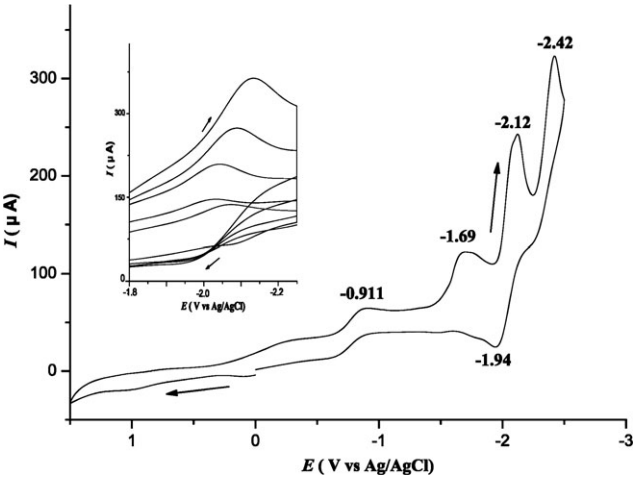

Fig. 7 Cyclic voltammogram (100 mV s^{-1}) for complex **1** in distilled MeCN. The inset is the curve of the scan rate dependence in the range 50–500 mV s^{-1}. The quoted potentials (V) are *vs.* Ag/AgCl.

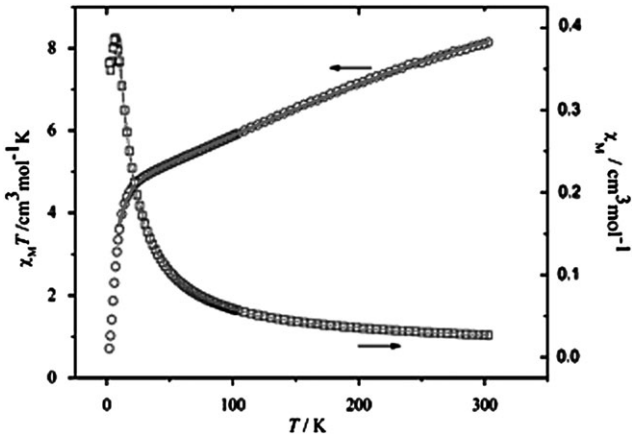

Fig. 8 Temperature dependence $\chi_M T$ (○) and χ_M (□) values for **1**. The solid lines correspond to the best-fit curves using the parameters described in the text.

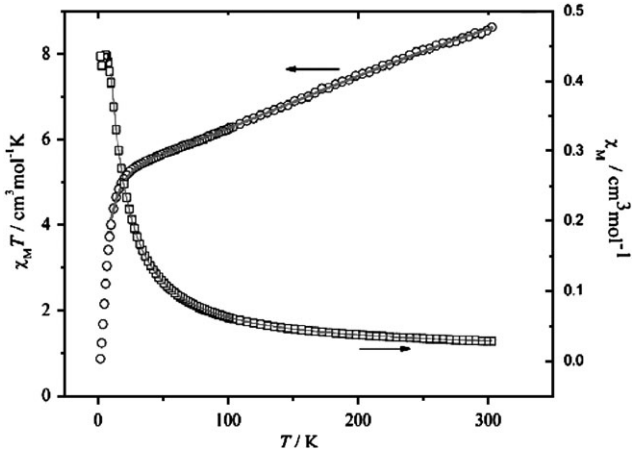

Fig. 9 Temperature dependence $\chi_M T$ (○) and χ_M (□) values for **3**. The solid lines correspond to the best-fit curves using the parameters described in the text.

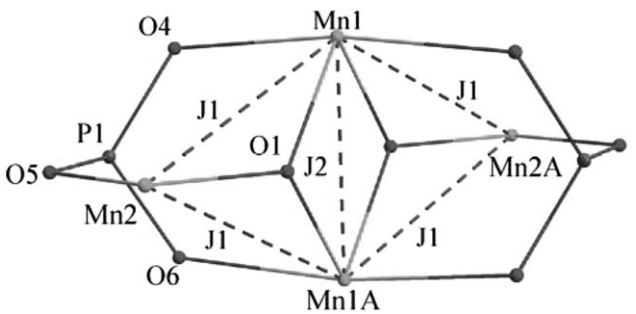

Fig. 10 The spin topology for **1** and **3** assuming two different J values.

20 K are $J_1 = -7.62$ cm^{-1}, $J_2 = -30.51$ cm^{-1}, $g = 2.18$, $zJ' = -0.6084$ and $R = 2.30728 \times 10^{-5}$ for **1** and $J_1 = -5.21$ cm^{-1}, $J_2 = -27.26$ cm^{-1}, $g = 2.04$, $zJ' = -0.58062$ and $R = 2.45243 \times 10^{-5}$ for **3**. The results reveal the overall antiferromagnetic character of the system, which are comparable to those tetranuclear Mn(III) complexes.[29,30] The results show the presence of antiferromagnetic interaction (J_2), which corresponds to the exchange interaction between the Mn(III) ions connected by two μ_3-O and two O–P–O bridges, and a weaker one (J_1), which corresponds to the exchange interaction between the Mn(III) ions connected by one μ_3-O, one O–C–O and one O–P–O bridges.

Thermal properties

The TGA curve of **1** (Fig. S6, ESI†) shows that the weight loss of 19.79 wt% from room temperature to 173 °C is due to the removal of four solvate MeCOOH molecules (calc. 19.54 wt%). On further heating (from 173 to 489 °C), the compound loses continuously 44.36 wt%, which corresponds to the loss of two bpy and four $MeCOO^-$ ligands (calc. 44.61 wt%). The compound does not lose any weight upon further heating to 1000 °C. As for compound **3** (Fig. S6, ESI†), it loses four solvate H_2O molecules at 78 °C with estimated weight loss of 5.35 wt% (calc. 5.84 wt%). On further heating, the compound loses 55.45 wt% continuously from 78 to 410 °C, which might be attributed to the release of one solvate $(COOH)_2$, two bpy and four $MeCOO^-$ ligands (calc. 51.76 wt%). The compound does not lose any weight after 560 °C.

Conclusions

In summary, we have explored the RPO_3H_2–Mn^{2+}–bpy/phen–MeCOOH/PhCOOH reaction system, and successfully prepared a family of new tetranuclear manganese(III) complexes **1–4** with different phosphonate ligands (RPO_3^{2-}, R = Me, Et and *n*-Bu) bicapping on the two sides of the $[Mn_4(\mu_3\text{-}O)_2]^{8+}$ core. Complexes **1** and **3** have been characterized by IR spectroscopy, ESI-MS spectrometry, electrochemical studies, magnetic measurements and TGA. More negative reduction potential values than the other reported manganese(III) complexes were observed. The electrochemical behaviors of compounds **1** and **3** reveal that this family of tetranuclear manganese(III) complexes are more difficult to be reduced. The results of the magnetic measurements indicate the antiferromagnetic interactions between the Mn(III) ions mediated through μ_3-O, O–C–O and O–P–O bridges. Further work is in progress to search for new manganese phosphonate clusters with interesting structures and magnetic properties.

Experimental

Materials

$Mn(O_2CPh)_2 \cdot 2H_2O$,[27] and $NBu^n_4MnO_4$[25] were both prepared according to the literature. All the other chemical reagents and solvents were of analytical grade and were purchased commercially and used without further purification.

Physical measurements

Elemental analyses (carbon, hydrogen and nitrogen) were performed using a vario EL III CHNOS elemental analyzer. Infrared spectra were recorded on a Nicolet magna 750 FT-IR spectrophotometer using KBr pellets in the range of 400–4000 cm^{-1}. Electrochemical studies were performed by a

CHI630A voltammetric analyzer. The auxiliary electrode was a Pt wire, the reference electrode an Ag/AgCl electrode and the working electrode a glassy carbon disk, which was carefully polished with gamma alumina powder (0.05 μm) before each voltammogram and then washed carefully with distilled acetonitrile. The measurement was recorded at room temperature in distilled MeCN solution under argon and 0.1 M $NBu^n_4PF_6$ was added as supporting electrolyte. Electrospray mass spectra were recorded in positive-ion mode with a DECAX-30000 LCQ Deca XP mass spectrometer. The variable-temperature susceptibility (2–300 K) was measured with a model PPMS60000 superconducting extraction sample magnetometer under a field of 0.5 T with the crystalline sample kept in a capsule for weighing. The thermogravimetric analysis was studied on a Mettler Toledo SDTA449c analyzer under nitrogen atmosphere.

Synthesis

$[Mn_4O_2(MePO_3)_2(O_2CMe)_4(bpy)_2]\cdot 4MeCOOH$ (1). To a stirred solution of $Mn(O_2CMe)_2\cdot 4H_2O$ (0.245 g, 1 mmol) and MeCOOH (7 mL, 0.122 mol) in MeCN (15 ml) was added solid $NBu^n_4MnO_4$ (0.091 g, 0.25 mmol) in small portions. To the resulting brown solution was added a solution of 2,2′-bipyridine (0.078 g, 0.5 mmol) and methanephosphonic acid ($MePO_3H_2$) (0.048 g, 0.5 mmol) in MeOH (5 ml) to yield a dark brown solution which was stirred for 24 h at room temperature, then filtered. The filtrate was left to stand at room temperature for about three weeks, during which time brown crystals were produced in 26% yield based on Mn. $C_{38}H_{50}Mn_4N_4O_{24}P_2$ (1228.52): calc. C 37.12, H 4.07, N 4.56; found C 37.07, H 4.12, N 4.62%. IR (KBr) data: $\tilde{\nu}$ = 3427 (s), 1720 (m), 1611 (m), 1566 (s), 1401 (s), 1069 (m), 1001 (m), 663 (w), 631 (w), 560 (w) cm^{-1}.

$[Mn_4O_2(EtPO_3)_2(O_2CMe)_4(bpy)_2]\cdot 7H_2O$ (2). The synthetic procedure of **1** was utilized to synthesize **2** with the use of ethanephosphonic acid ($EtPO_3H_2$) instead of methanephosphonic acid ($MePO_3H_2$). Brown crystals were obtained in 22% yield based on Mn. $C_{32}H_{52}Mn_4N_4O_{23}P_2$ (1142.48): calc. C 33.61, H 4.55, N 4.90; found C 33.69 H 4.49 N 4.86%. IR (KBr) data: $\tilde{\nu}$ = 2967 (w), 2933 (w), 1583 (s), 1446 (m), 1399 (s), 1337 (m), 1082 (w), 1015 (w), 943 (s), 665 (m), 654 (w), 629 (w) cm^{-1}.

$[Mn_4O_2(n\text{-}BuPO_3)_2(O_2CMe)_4(bpy)_2]\cdot 4H_2O\cdot(COOH)_2$ (3). This complex was obtained using a procedure similar to that used for preparing **1**, except that 1-butanephosphonic acid (n-$BuPO_3H_2$) was used instead of methanephosphonic acid ($MePO_3H_2$) and a mixture of MeCOOH (7 mL, 0.122 mol) and $(COOH)_2\cdot 2H_2O$ (0.0126 g, 0.1 mmol) instead of MeCOOH. Brown crystals were obtained in 20% yield based on Mn. $C_{38}H_{60}Mn_4N_4O_{24}P_2$ (1232.55): calc. C 36.99, H 4.87, N 4.54; found C 36.20, H 4.61, N 4.25%. IR (KBr) data: $\tilde{\nu}$ = 3417 (s), 2954 (m), 1737 (m), 1579 (s), 1498 (w), 1400 (s), 1338 (s), 1085 (s), 1001 (s), 1001 (s), 950 (s), 666 (w) cm^{-1}.

$[Mn_4O_2(MePO_3)_2(O_2CPh)_4(phen)_2]\cdot 4PhCOOH\cdot 2CH_3CN$ (4). To a stirred solution of $Mn(O_2CPh)_2\cdot 2H_2O$ (0.333 g, 1 mmol) and PhCOOH (1.22 g, 10 mmol) in 2 : 1 CH_2Cl_2–MeCN (15 ml) was added solid $NBu^n_4MnO_4$ (0.091 g, 0.25 mmol) in small portions. To the resulting brown solution was added a solution of 1,10-phenanthroline (0.10 g, 0.5 mmol) and methanephosphonic acid ($MePO_3H_2$) (0.048 g, 0.5 mmol) in MeOH (5 ml) to yield a dark brown solution which was stirred for 24 h at room temperature, then filtered. The filtrate was left to stand at room temperature for about three weeks, during which time brown crystals were deposited in 21% yield based on Mn. $C_{86}H_{72}Mn_4N_6O_{24}P_2$ (1855.20): calc. C 55.63, H 3.88, N 4.53; found C 55.58, H 3.82, N 4.59%. IR (KBr) data: $\tilde{\nu}$ = 3851 (s), 3748 (m), 3673 (s), 3650 (s), 3065 (s), 1704 (s), 1599 (s), 1555 (s), 1520 (m), 1449 (m), 1430 (m), 1401 (s), 1385 (s), 1313 (w), 1248 (m), 1110 (w), 1046 (w), 1020 (m), 996 (m), 954 (m), 716 (s) cm^{-1}.

Crystallographic determinations

The diffraction data for complexes **1–4** were collected at 293(2) K on a mercury-CCD/AFCR diffractometer with Mo-Kα radiation (λ = 0.71073 Å). Empirical absorption correction was applied by using SADABS program.[37] All the structures were solved by direct methods and refined by full-matrix least-squares techniques based on F^2 with all observed reflections, performed with SHELXTL-97 package.[38] The non-hydrogen atoms were refined anisotropically. The hydrogen atoms were located by geometrically calculations except for those on the water molecules which were located from the difference Fourier syntheses. Six DFIX instructions were applied to restrain bond distances of solvate water molecules of compound **2**. Five restraints of DFIX instructions were used to improve the geometry of the distorted solvate oxalic acid molecular in compound **3**, and the O14–O15–C19–C20-O16–O17 unit (r.m.s. deviation 0.0010 Å) was restrained to be flat by the FLAT 0.01 instruction (three restraints).

CCDC reference numbers 635082–635085.

For crystallographic data in CIF or other electronic format see DOI: 10.1039/b706514k

Acknowledgements

This work was supported by the National Natural Science Foundation of China (No. 20471061 and No. 20633020) and the Science & Technology Innovation Foundation for the Young Scholar of Fujian Province (No. 2005J059).

References

1 (*a*) J. Amesz, *Biochim. Biophys. Acta*, 1983, **726**, 1; (*b*) G. C. Dismukes, *Photochem. Photobiol.*, 1986, **43**, 99.
2 A. Zouni, H.-T. Witt, J. Kern, P. Fromme, N. Krauss, W. Saenger and P. Orth, *Nature*, 2001, **409**, 739.
3 D. Gatteschi and R. Sessoli, *Angew. Chem., Int. Ed.*, 2003, **42**, 268.
4 J. Tejada, E. M. Chudnovsky, E. del Barco, J. M. Hernandez and T. P. Spiller, *Nanotechnology*, 2001, **12**, 181.
5 B. Zhou, R. Tao, S.-Q. Shen and J.-Q. Liang, *Phys. Rev. A*, 2002, **66**, 010301(R).
6 J. R. Friedman, M. P. Sarachik, J. Tejada and R. Ziolo, *Phys. Rev. Lett.*, 1996, **76**, 3830.
7 L. Thomas, F. Lionti, R. Ballou, D. Gatteschi, R. Sessoli and B. Barbara, *Nature*, 1996, **383**, 145.
8 E. K. Brechin, R. A. Coxall, A. Parkin, S. Parsons, P. A. Tasker and R. E. P. Winpenny, *Angew. Chem., Int. Ed.*, 2001, **40**, 2700.
9 S. Y. Song, J. F. Ma, J. Yang, M. H. Cao and K. C. Li, *Inorg. Chem.*, 2005, **44**, 2140.

10 B. Bujoli, S. M. Lane, G. Nonglaton, M. Pipelier, J. Léger, D. R. Talham and C. Tellier, *Chem.–Eur. J.*, 2005, **11**, 1980.
11 K. Maeda, *Microporous Mesoporous Mater.*, 2004, **73**, 47.
12 A. K. Cheetham, G. Férey and T. Loiseau, *Angew. Chem., Int. Ed.*, 1999, **38**, 3268.
13 M. I. Khan and J Zubieta, *Prog. Inorg. Chem.*, 1995, **43**, 1, and references therein.
14 M. G. Walawalkar and H. W. Roesky, *Acc. Chem. Res.*, 1999, **32**, 117, and references therein.
15 V. Chandrasekhar and S. Kingsley, *Angew. Chem., Int. Ed.*, 2000, **39**, 2320.
16 D.-K. Cao, Y.-J. Liu, Y. Song and L.-M. Zheng, *New J. Chem.*, 2005, **5**, 721.
17 V. Chandrasekhar, S. Kingsley, B. Rhatigan, M. K. Lam and A. L. Rheingold, *Inorg. Chem.*, 2002, **41**, 1030.
18 J.-G. Mao, Z. Wang and A. Clearfiled, *New J. Chem.*, 2002, **26**, 1010.
19 G. Anantharaman, M. G. Walawalker, R. Murugavel, B. Gabor, R. Herbst-Irmer, M. Baldus, B. Angerstein and H. W. Roesky, *Angew. Chem., Int. Ed.*, 2003, **42**, 4482.
20 E. I. Tolis, M. Helliwell, S. Langley, J. Raftery and R. E. P. Winpenny, *Angew. Chem., Int. Ed.*, 2003, **42**, 3804.
21 S. Maheswaran, G. Chastanet, S. J. Teat, T. Mallah, R. Sessoli, W. Wernsdorfer and R. E. R. Winpenny, *Angew. Chem., Int. Ed.*, 2005, **44**, 5044.
22 H.-C. Yao, Y.-Z. Li, Y. Song, Y.-S. Ma, L.-M. Zheng and X.-Q. Xin, *Inorg. Chem.*, 2006, **45**, 59.
23 Y.-S. Ma, H.-C. Yao, W.-J. Hua, S.-H. Li, Y.-Z. Li and L.-M. Zheng, *Inorg. Chim. Acta*, 2007, **360**, 1645.
24 J. B. Vincent, H.-R. Chang, K. Folting, J. C. Huffman, G. Christou and D. N. Hendrickson, *J. Am. Chem. Soc.*, 1987, **109**, 5703.
25 J. B. Vincent, K. Folting, J. C. Huffman and G. Christou, *Inorg. Chem.*, 1986, **25**, 996.
26 W. T. Liu and H. H. Thorp, *Inorg. Chem.*, 1993, **32**, 4102.
27 E. Libby, J. K. McCusker, E. A. Schmitt, K. Folting, D. N. Hendrickson and G. Christou, *Inorg. Chem.*, 1991, **30**, 3486.
28 S. Wang, M. S. Wemple, J. Yoo, K. Folting, J. C. Huffman, K. S. Hagen, D. N. Hendrckson and G. Christou, *Inorg. Chem.*, 2000, **39**, 1501.
29 C. Cañada-Vilalta, J. C. Huffman and G. Christou, *Polyhedron*, 2001, **20**, 1785.
30 P. Chaudhuri, E. Rentschler, F. Birkelbach, C. Krebs, E. Bill, T. Weyhermüller and U. Flörke, *Eur. J. Inorg. Chem.*, 2003, 541.
31 G. Christou and J. B. Vincent, in *ACS Symposium Series 372*, ed. L. Que, American Chemical Society, Washington DC, 1988, ch. 12, pp. 238–255.
32 A. R. E. Baikie, M. B. Hursthouse, D. B. New and P. Thornton, *J. Chem. Soc., Chem. Commun.*, 1978, 62.
33 A. R. E. Baikie, M. B. Hursthouse, L. New, P. Thornton and R. G. White, *J. Chem. Soc., Chem. Commun.*, 1980, 684.
34 E. Bouwman, M. A. Bolcar, E. Libby, J. C. Huffman, K. S. Hagen and G. Christou, *Inorg. Chem.*, 1992, **31**, 5185.
35 A.-L. Barra, D. Gatteschi, R. Sessoli, G. L. Abbati, A. Cornia, A. C. Fabretti and M. G. Uytterhoeven, *Angew. Chem., Int. Ed. Engl.*, 1997, **36**, 2329.
36 χ_0 is the susceptibility of the noninteracting compounds, z is the number of nearest neighbors and J' is the magnetic interactions between units. See: C. Kachi-Terajima, H. Miyasaka, K.-i. Sugiura, R. Clérac and H. Nojin, *Inorg. Chem.*, 2006, **45**, 4381.
37 G. M. Sheldrick, *SADABS Software for Empirical Absorption Correction*, University of Göttingen, Germany, 1996.
38 G. M. Sheldrick, *SHELXTL*, Structure Determination Software Programs, Bruker Analytical X-ray System Inc., Madison WI, 1997.

